Determination of the quark-antiquark potential in the Hamiltonian formulation of the compact U(1) gauge theory.

Angelo Brade

Rheinische Friedrich–Wilhelms–Universität, Bonn.

Contributing authors: s72abrad@uni-bonn.de;

Ich versichere, dass ich diese Arbeit selbstständig verfasst und keine anderen als die angegebenen Quellen und Hilfsmittel benutzt sowie die Zitate kenntlich gemacht habe.

Bonn, ...,
            Datum   Unterschrift

1. Gutachter: Prof. Dr. Carsten Urbach
2. Gutachterin: Prof. Dr. Lena Funcke

Contents

1 Abstract

For this work, a lattice will be constructed in the compact U(1) theory within pure gauge. It will give an insight in the implementation using `Python`. One intention of this work is to give a good introduction such that other new students of the compact U(1) theory will have a better understanding and intuition. The setup will be truncated appropriately and reduced from the complete configuration space to a physical configuration space through Gauss's Law. For the numerical results, the expectation value for the plaquette operator and the $q\bar{q}$ potential is determined. For the latter, confinement will be shown. Furthermore the variation of the lattice properties, such as truncation l, coupling g and positioning of the quarks will be discussed.

2 Introduction

The Hamiltonian formulation of lattice gauge theory was first regarded as too costly for reasonable calculations. With the advent of quantum computers a significant speedup of calculations, that can be represented with states, is expected. The use of entanglement of these states promises an exponential improvement. This property gives quantum devices the ability to efficiently calculate lattices in the Hamiltonian formulation.[1, 2] Another effective method are tensor networks, which can be used on classical computers. Independent of the implementation, the Hamiltonian formulation on the lattice is a crucial tool to do calculations, where the Markov chain Monte Carlo (MCMC) simulations of the Lagrangian formulation fails, due to the sign problem.[3] This fact moves the Hamiltonian formulation in a point of interest again. For that reason this work will revisit this formulation and implement the theory on a classical computer using the most basic method of exact diagonalization.

In the U(1) theory, the only properties of particles are their masses and their charges. Since this work will only focus on pure gauge, there are no fermionic fields, i.e no kinetic properties. This renders the mass obsolete and the only defining property left is the charge. Therefore quarks and antiquarks can be represented solely by a point-like charge.

When working on a pure gauge lattice the physical scale and thus the units are lost. Since this is a $(2 + 1)$ dimensional theory, i.e. two space and one time dimension, the unit scale can not be recovered. For this a $(3 + 1)$ dimensional theory is needed, such that experimental results can be matched with theoretical results from the lattice. This way the lattice spacing a, and thus the unit scale, can be determined.

3 Theory

3.1 *Discretization*

The positional space is discretized into a lattice with sites that are connected by links. Sites are spaced by the lattice spacing a. To obtain the continuum theory in the limit of $a \rightarrow 0$, the coupling constant g is introduced.[4]

Each site is associated with a corresponding positional vector $\vec{r} = (r_x, r_y) \in \mathbb{Z}^{n_x \times n_y}$ for a $n_x \times n_y$ lattice. On the sites are the static charges $Q_{\vec{r}}$ positioned. Each link is associated with a corresponding position $\vec{r}$ and a direction μ, where $-\mu$ is its opposite direction. For example, the link that points from the site $(1, 2)$ to the x direction is denote with $\vec{r} = (1, 2)$ and $\mu = x$. The same link is denoted with $\vec{r} = (2, 2)$ and $\mu = -x$.

On the links are the electric field operators $\hat{E}_{\vec{r},\mu}$ positioned. Each electric field $\hat{E}_{\vec{r},\mu}$ has the vector potential $\hat{A}_{\vec{r},\mu}$ as its canonical conjugate variable. Thus,

$$[\hat{E}_{\vec{r}_i,\mu}, \hat{A}_{\vec{r}_j,\nu}] = i\delta^{(3)}(\vec{r}_i - \vec{r}_j)\delta_{\mu\nu}. \qquad (1)$$

A unitary operator $\hat{U}_{\vec{r}_j,\nu}$, also referred to as the link operator, is constructed using the vector potential as the generator in the Lie algebra $\mathfrak{g}$. Through the exponential map, this yields elements of the associated Lie group G:

$$\hat{U}_{\vec{r},\mu} = e^{iag\hat{A}_{\vec{r},\mu}}. \qquad (2)$$

The generated Lie group $G = U(n)$ has the complex matrix elements $\hat{U}_{\vec{r},\nu}$ of dimension $n \times n$. The U(1) theory is chosen by taking $n = 1$. Restricting $\hat{A}_{\vec{r},\mu}$ to $ag\hat{A}_{\vec{r},\mu} \in [0, 2\pi)$, provides the compact U(1) theory. Through Equations (1) to (2) the following relation is obtained:

$$[\hat{E}_{\vec{r}_i,\mu}, \hat{U}_{\vec{r}_j,\nu}] = \delta^{(3)}(\vec{r}_i - \vec{r}_j)\delta_{\mu\nu}\hat{U}_{\vec{r}_j,\nu}, \qquad (3)$$

$$[\hat{E}_{\vec{r}_i,\mu}, \hat{U}^{\dagger}_{\vec{r}_j,\nu}] = -\delta^{(3)}(\vec{r}_i - \vec{r}_j)\delta_{\mu\nu}\hat{U}^{\dagger}_{\vec{r}_j,\nu}. \qquad (4)$$

To explore the effect of the operators on the states, the electric basis with the basis states $|e_{\vec{r},\mu}\rangle$ is chosen. The basis is made up of all possible states at the links. Thus,

$$\hat{E}_{\vec{r},\mu}|e_{\vec{r},\mu}\rangle = e_{\vec{r},\mu}|e_{\vec{r},\mu}\rangle. \qquad (5)$$

Furthermore Equations (3) to (5) give rise to

$$\hat{U}_{\vec{r},\mu}|e_{\vec{r},\mu}\rangle = |e_{\vec{r},\mu} + 1\rangle \text{ and} \qquad (6)$$

$$\hat{U}^{\dagger}_{\vec{r},\mu}|e_{\vec{r},\mu}\rangle = |e_{\vec{r},\mu} - 1\rangle. \qquad (7)$$

This means, the link operators act as ladder operators.

3.2 Truncation

Since each field can take any real value, there are infinite many possible values for each link, thus constructing an infinite basis. To be computable, possible values are truncated, such that the basis is finite. Truncating means, doing calculations only to an finite order.

Revisiting U(1), shows that is homeomorphic to S^1, i.e. the unit circle on the complex plane. By limiting the phase of the exponential mapping in equation Equation (2) to $[-l, l]$, the phase is now an element of $\mathbb{Z}_{2l+1}$. This also truncates the electric field, such that

$$e_{\vec{r}_i,\mu} \in [-l, l]. \qquad (8)$$

The link operators, which act as ladder operators on the eigenstates, can now also be expressed as

$$\hat{U}_{\vec{r},\mu} \mapsto \begin{bmatrix} 0 & \dots & \dots & 0 \\ 1 & \dots & \dots & 0 \\ 0 & \ddots & \vdots & 0 \\ 0 & \dots & 1 & 0 \end{bmatrix}, \hat{U}^{\dagger}_{\vec{r},\mu} \mapsto \begin{bmatrix} 0 & 1 & \dots & 0 \\ 0 & \vdots & \ddots & 0 \\ 0 & \dots & \dots & 1 \\ 0 & \dots & \dots & 0 \end{bmatrix}.$$

The unitarity $\hat{U}_{\vec{r},\mu}\hat{U}^{\dagger}_{\vec{r},\mu} \neq \mathbb{1}$ for this is lost, but can be recovered in the continuum limit of $a \to 0$. It is important to point out, that the first (last) state is annihilated when using $\hat{U}^{\dagger}_{\vec{r}}$ ($\hat{U}_{\vec{r}}$).

3.3 *Hamiltonian*

The Hamiltonian for lattice gauge theory was originally formulated by Kogut and Susskind [5] and therefore since known as the so called Kogut Susskind Hamiltonian. It reads

$$\hat{H} = \hat{H}_E + \hat{H}_B + \hat{H}_m + \hat{H}_{\text{kin}} \text{ with}$$

$$\hat{H}_E = \frac{g^2}{2} \sum_{\vec{r}} \left(\hat{E}^2_{\vec{r},x} + \hat{E}^2_{\vec{r},y} \right),$$

$$\hat{H}_B = -\frac{1}{a^2 g^2} \sum_{\vec{r}} \text{Re}(\text{Tr}(\hat{P}_{\vec{r}})),$$

$$\hat{H}_m = m \sum_{\vec{r}} (-1)^{r_x + r_y} \hat{\phi}^{\dagger}_{\vec{r}} \hat{\phi}_{\vec{r}} \text{ and}$$

$$\hat{H}_{\text{kin}} = \frac{i}{2a} \sum_{\vec{r}} \left(\phi^{\dagger}_{\vec{r}} \hat{U}_{\vec{r},x} \phi_{\vec{r}+x} - \text{h.c.} \right)$$

$$- \frac{(-1)^{r_x + r_y}}{2a} \sum_{\vec{r}} \left(\phi^{\dagger}_{\vec{r}} \hat{U}_{\vec{r},y} \phi_{\vec{r}+y} + \text{h.c.} \right).$$

At the beginning the static charges $Q_{\vec{r}}$ were introduced. They are called static, since they can not move and thus have no field. In the physical context they have infinite mass. Therefore the fermionic fields $\hat{\phi}_{\vec{r}}$ vanish at all $\vec{r}$. This premiss yields

$$\hat{H}_m = \hat{H}_{\text{kin}} = 0.$$

The computation can also be done with dynamic charges $\hat{q}_{\vec{r}}$ where the mass and kinetic Hamiltonian will contribute. In this case a phenomenon called the doubling problem will rise. A common approach for this problem is staggered fermions. This will not be looked into further. Instead the, pure gauge case is used, where only gauge fields exist.

Only the electric Hamiltonian $\hat{H}_E$ and the magnetic Hamiltonian $\hat{H}_B$ contribute. For the latter one, the plaquette operator $\hat{P}_{\vec{r}}$ is introduced. A plaquette is the smallest Wilson loop (a closed loop through the lattice on the link operators) and the corresponding operator is formed by the

oriented product of the link operators, i.e.

$$\hat{P}_{\vec{r}} = \hat{U}_{\vec{r},x} \hat{U}_{\vec{r}+x,y} \hat{U}_{\vec{r}+y,x}^{\dagger} \hat{U}_{\vec{r},y}^{\dagger}, \tag{9}$$

where e.g. $\vec{r} + x = (r_x + 1, r_y)$. The hermitian conjugates of the two latter link operators are used since all link operators are oriented towards the positive x or y direction and when looping around the plaquette, the direction is against the orientation of the two last link operators. Since the link operators are 1×1 matrices, the trace is just its argument. Taking the real part of an operator is not intuitive, so it is rewritten with the definition of the real part as

$$\text{Re}(\hat{P}_{\vec{r}}) = \frac{\hat{P}_{\vec{r}} + \hat{P}_{\vec{r}}^{\dagger}}{2}. \tag{10}$$

The hermitian conjugate of the plaquette operator is the same as reversing the direction of the loop.

The heuristic explanation of the form of the magnetic Hamiltonian is the following: plaquettes, as they are closed loops, are essentially conductor loops which introduce a magnetic moment, that is then measured by the magnetic Hamiltonian. This analogy is not a rigorous argument, but rather shall help build a first intuition.

The electric Hamiltonian is essentially the sum over each lattice site over the square of the electric field. Here the electric field operators $\hat{E}_{\vec{r},\mu}$ are being used and no modifications have to be made, since the electric operator is diagonal in the electric basis.

Finally, the total Hamiltonian reads

$$\hat{H} = \frac{g^2}{2} \sum_{\vec{r}} \left(\hat{E}_{\vec{r},x}^2 + \hat{E}_{\vec{r},y}^2 \right) - \frac{1}{2a^2 g^2} \sum_{\vec{r}} \left(\hat{P}_{\vec{r}} + \hat{P}_{\vec{r}}^{\dagger} \right).$$

3.4 Gauss's law

A constraint that limits the possible states is Gauss's law. It constraints by the number of lattice sites, such that some links are dependent on other links. Links that are dependent on other links are called fixed links. While links that are independent are called dynamic links. This can be formulated as

$$\left[\sum_{\mu=x,y} \left(\hat{E}_{\vec{r},\mu} - \hat{E}_{\vec{r}-\mu,\mu} \right) - Q_{\vec{r}} \right] |\Psi\rangle = 0. \tag{11}$$

The law promises, that the sum over all electric field operators that are linked to a site $\vec{r}$ is equal to the charge deposited on the site. Only those lattice states $|\Psi\rangle$, which produce this relation, are thus physically possible. They live in the physical space $\mathcal{H}_{\text{ph}}$:

$$|\Psi\rangle \in \mathcal{H}_{\text{ph}}, \tag{12}$$

where $\mathcal{H}$ denotes the space in which a lattice configuration lives. Here the physical configuration Hamiltonian $\mathcal{H}_{\text{ph}}$ is a subspace of the complete configuration Hamiltonian $\mathcal{H}$.

The dependence on the fixed links is used to represent them in terms of the dynamic links. This can by done analytically on paper or with the library sympy[6] in python. For convenience, the latter is used. This way the generated linear system of equations is solved.

4 Implementation

The code for this work can be accessed via GitHub: https://github.com/valentino-dev/Bachelorthesis/tree/main/src.

4.1 Matrix representation

For the implementation, the lattice is constructed and all operators are placed on their links. Then each entry is calculated:

$$\langle i | \hat{H} | j \rangle = \frac{g^2}{2} \sum_{\vec{r}} \left(e_{\vec{r},x}^2 + e_{\vec{r},y}^2 \right) \delta_{ij}$$
$$- \frac{1}{2a^2 g^2} \sum_{\vec{r}} \langle i | \left(\hat{P}_{\vec{r}} + \hat{P}_{\vec{r}}^{\dagger} \right) | j \rangle$$

with $|i\rangle \in \mathcal{H}$. Starting with $\langle i | \hat{P}_{\vec{r}} | j \rangle$:

$$\langle i | \hat{P}_{\vec{r}} | j \rangle = \langle i | \hat{U}_{\vec{r},x} \hat{U}_{\vec{r}+x,y} \hat{U}_{\vec{r}+y,x}^{\dagger} \hat{U}_{\vec{r},y}^{\dagger} | j \rangle$$
$$= \langle i | (|e_{\vec{r},x}^{(j)} + 1\rangle \otimes |e_{\vec{r}+x,y}^{(j)} + 1\rangle$$
$$\otimes |e_{\vec{r}+y,x}^{(j)} - 1\rangle \otimes |e_{\vec{r},y}^{(j)} - 1\rangle$$
$$\bigotimes_{\text{rest links}} |e_{\vec{r}',\mu'}^{(j)}\rangle)$$
$$= \langle i \,|\, k \rangle$$
$$= \delta_{ik}$$

The formulation reads as following: State $|j\rangle$ will be transformed by the plaquette operator $\hat{P}_{\vec{r}}$ into

some state $|k\rangle$. Thus $\hat{P}_{\vec{r}}$ gets an entry at row $\langle i|$ and column $|j\rangle$ if, and only if, state $|j\rangle$ is transformed into state $|i\rangle$.

Now knowing $\hat{P}_{\vec{r}}$ in matrix representation, trivially yields $\hat{P}_{\vec{r}}^{\dagger} = \left(\hat{P}_{\vec{r}}^{*}\right)^{T}$ and with it the matrix representation of the magnetic Hamiltonian.

On a side note, going through states $|i\rangle$ means, counting up in base $2l + 1$ with the link states $|e_{\vec{r},\mu}\rangle$ being the "digits". This is schematically illustrated in Table 1.

i	$\|i\rangle = \|e_0^{(j)}, e_1^{(j)}, \ldots, e_{N_1-2}^{(j)}, e_{N_1-1}^{(j)}\rangle$
0	$\|-l, -l, \ldots, -l, -l\rangle$
1	$\|-l, -l, \ldots, -l, -l+1\rangle$
$\vdots$	$\vdots$
$2l$	$\|-l, -l, \ldots, -l, l\rangle$
$2l + 1$	$\|-l, -l, \ldots, -l+1, -l\rangle$
$\vdots$	$\vdots$
$(2l+1)^{N_1} - 2$	$\|l, l, \ldots, l, l-1\rangle$
$(2l+1)^{N_1} - 1$	$\|l, l, \ldots, l, l\rangle$

Table 1: Scheme of state indexing with $N_1 :=$ number of links and $e_m^{(j)}$ being the value for link $m \in [0, N_1 - 1]$ (m is bijective to $((x, y), \mu)$) in lattice configuration $j \in [0, (2l+1)^{N_1}]$.

With this procedure every combination of states $\langle i|$ and $|j\rangle$ would have to be checked, which would be very costly. Instead just the transformation $\hat{P}_{\vec{r}} |j\rangle = |k\rangle$ is calculated for every state $|j\rangle$ and set $(\hat{P}_{\vec{r}})_{kj} = 1$, i.e. having a contribution at row $\langle k|$ and column $|j\rangle$.

Gauss's Law not only restricts the electric operators, but also the corresponding link operator on the same link. But here Gauss's Law does not impose a dependency, but rather the dynamical link operators automatically produce physical states, where as the fixed link operators do not act on our physical space anymore, which is why the fixed ones are ignored. With plaquette operators there are normally always four link operators, where as now the plaquette operators are a product of any number of link operators ranging from 0 to 4. Which number it will be is then dependent on the position of the plaquette, i.e. the number of dynamical links it loops through. When a plaquette does not go through any dynamical link operators, it will never produce a physical state and thus can be ignored entirely.

4.2 Exact diagonalization

Now having the total Hamiltonian in matrix representation, diagonalization is used to compute the eigenvalues and eigenstates. For this the library `scipy` [7] is used. It provides the method `scipy.sparse.linalg.eigsh`, which is an eigensolver and can be used to calculate the k smallest algebraic (SA) eigenvalues. It uses hermitian sparse row matrices, which speed up the process drastically in comparison to dense non hermitian matrices.

Alternatively, instead of exact diagonalization, one could use tensor networks, or on a quantum computer, a variational quantum eigensolver (VQE).

4.3 Computational resources

The disadvantage of the Hamiltonian formulation of the lattice gauge theory, that is its need for computational resources,[1] since every link can be in $2l + 1$ states and in two dimensions, there are two links for every site. Now depending if periodic boundary conditions (PBC) are being used or not, there are links that connect the sites of opposite sides or not. The exact number of states for a square $n \times n$ lattice with PBC would be $N = (2l+1)^{2n^2}$ and without PBC $N = (2l+1)^{2(n^2-n)}$. Only physical states are of interest. Using Gauss's Law imposes constraints and thus restricts the number of total states to only the physical states. So each site introduces a constraint

$$\sum_{\mu=x,y} \left(\hat{E}_{\vec{r},\mu} - \hat{E}_{\vec{r},-\mu}\right) |\Psi\rangle = Q_{\vec{r}} |\Psi\rangle. \qquad (13)$$

To check if they are linearly independent, Gauss's Law of all sites is summed up:

$$\sum_{\vec{r}} \sum_{\mu=x,y} \left(\hat{E}_{\vec{r},\mu} - \hat{E}_{\vec{r},-\mu}\right) |\Psi\rangle = \sum_{\vec{r}} Q_{\vec{r}} |\Psi\rangle. \qquad (14)$$

Only if the total sum of charges is non zero, linear independency is given. But if the total sum is zero, a redundant constraint arises, which reduces the total number of constraints from n^2 to $n^2 - 1$. From now on the total charge is always zero, since only lattices with no charges or with a pair of opposite charges are considered.

This limits our total number of electric operators $N_E = 2n^2$ to only a fraction that is dynamic:

$N_{E,\mathrm{dyn}} = n^2 + 1$. A lattice without PBC has $N_E = 2(n^2 - n)$ and $N_{E,\mathrm{dyn}} = n^2 - 2n + 1$. The number of physical states for a lattice with PBC is thus

$$N_{\mathrm{ph}} = (2l + 1)^{n^2+1}. \tag{15}$$

And without PBC

$$N_{\mathrm{ph}} = (2l + 1)^{n^2-2n+1} \tag{16}$$

$$= (2l + 1)^{(n-1)^2} \tag{17}$$

On a side note, Equation (17) shows, that a $n \times n$ lattice without PBC has just as many links as a lattice with $(n-1) \times (n-1)$ lattice with PBC. Since from the calculations, matrices with size $N_{\mathrm{ph}} \times N_{\mathrm{ph}}$ are returned, the number of physical states will be a good measure for computation time. To get an idea on some realistic lattices and their number of physical states, see Table 2.

lattice	N_{ph}
2×2, no PBC and $l = 1$	3
2×2, PBC and $l = 1$	243
2×2, PBC and $l = 7$	759×10^3
3×3, PBC and $l = 1$	59.1×10^3
3×3, PBC and $l = 2$	9.77×10^6
3×3, PBC and $l = 3$	283×10^6
3×3, PBC and $l = 4$	3.49×10^9

Table 2: Lattice sizes and their number of physical states.

An advantage is, that most of the elements of the Hamiltonian are zero and only a few are non-zero entries. Thus instead of storing all elements, even those that are zero, only the non-zero entries are being stored by row position, column position and the value. This is called a Compressed Sparse Row (CSR) matrix and will reduce the needed memory drastically.[1]

Now that a little intuition for the complexity is obtained, the next step is to continue with the actual computation times. This work will not go into the detail of time complexity, but rather use first hand measurements. The calculations are done on the high performance computing (HPC) cluster

---

[1] Nevertheless a Hamiltonian of a 3×3 lattice with PBC and $l = 3$ takes about $150\,\mathrm{GB}$ to be stored.

Marvin of the University of Bonn. Three computation times are listed in Table 3.[2] Table 3 confirms

truncation l	building $\hat{H}$	diagonalizing
1	$1.5\,\mathrm{s}$	$0.27\,\mathrm{s}$
2	$110\,\mathrm{s}$	11 minutes
3	$1\,\mathrm{h}$	$5\,\mathrm{h}$

Table 3: Computation time for a 3×3 lattice with PBC.

the problem, that computation times grow rapidly, and large scale computations are not feasible on classical hardware.

To utilize the HPC to capacity, multiprocessing was introduced. The code was rewritten, such that the calculation of the elements are distributed onto the threads, without distributing to thinly, i.e. launching new threads takes more time then processing, or to dense, i.e. not all cores are utilized.

5 Results

5.1 *Plaquette expectation value*

As first comparison and confirmation of the presented setup, the plaquette expectation value are of interest. It is defined as the following:

$$\langle P \rangle = \left\langle \sum_{\vec{r}} \frac{P_{\vec{r}} + P_{\vec{r}}^{\dagger}}{2} \right\rangle. \tag{18}$$

From the scaling of the Hamiltonian in respect to g, $\lim_{g \to \infty} \langle P \rangle = 0$ and $\lim_{g \to 0} \langle P \rangle = 1$ are expected. This behaviour is intuitive, when thinking of the plaquette expectation value as a measure of the contribution from the plaquette operator to the Hamiltonian. Since the electric Hamiltonian is proportional to g^2, it should dominate for strong couplings. For weak couplings, the magnetic Hamiltonian is expected to dominate, and thus the plaquette operator, since it is proportional to $1/g^2$. When comparing this expectation to the following results, one has always to be mindful of the fact, that the x-axis shows $\beta = 1/g^2$.

Figure 1 is the result of the calculation, confirming the expected. An interesting but not

---

[2] This assessment was done by using one node with two CPUs of the type Intel Xeon 'Sapphire Rapids' 48-core/96-thread 2.10GHz.
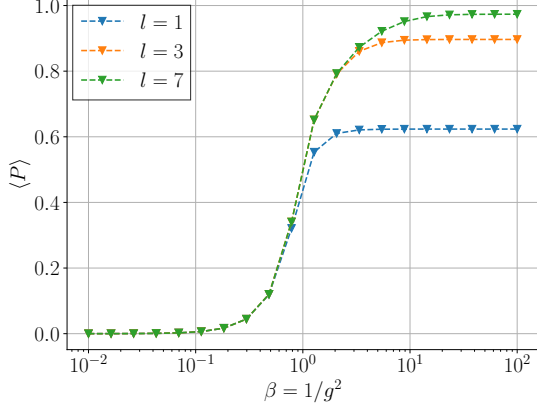
Figure 1: plaquette expectation values for a 2×2 lattice with PBC.

surprising observation is the convergence of the expectation value to 1 for large β with the order of truncation. This is due to the approach to continuum theory for large truncations. Thus using large l is favourable.

As a next step, larger lattices of dimensions 3×3 are calculated. Figure 2 shows the results. The linear scale and range of β is chosen, to be comparable to fig. 5 from Arianna Crippa et al. (2024)[8].
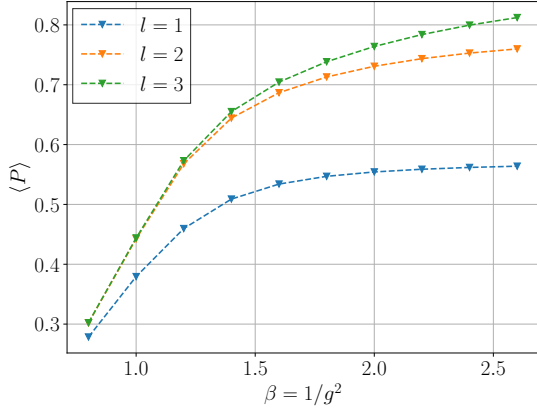
Figure 2: Plaquette expectation values for a 3×3 lattice with PBC.

It again confirms the convergence to 1 with increasing β and weakening truncation. Weak truncation meaning larger l, since for infinite l the truncation effect would vanish.

5.2 *Quark-Antiquark potential*

Now for calculating the quark antiquark potential, the energy of the chargeless lattice $\hat{H}_0$ is subtracted:

$$V = \langle \hat{H} \rangle - \langle \hat{H}_0 \rangle \tag{19}$$

with $\hat{H}$ being the lattice with the desired charge. This reduces the total energy to the potential energy emitted by the charge and renormalizes it when approaching continuum theory. For the purpose of this work, one charge is being placed in the bottom left corner and the opposite charge at a lattice site with desired distance. The study of the effect of different setups on charge pairs with the same distance is also of interest. Thus the truncation l is varied from 1 to 3 and compared to the original 3×3 lattice with no PBC, with PBC and a lattice with dimensions 4×4. With these different setups Figure 3 is obtained. Throughout this section this is the central Figure, that is discussed.

The most basic setup is a 3×3 lattice with no PBC and a truncation of $l = 1$. The potential raises linearly with increasing distance

$$V(r) = \sigma r, \tag{20}$$

where σ is the so called string tension. From a classical perspective this is surprising. But this phenomena has already been reviewed [4] and it is indeed confinement.

Now different lattice parameters are varied. Starting with a different truncation l, here 2 and 3, the potential has the same behaviour, but is more linear. This shows, that indeed the truncation effects vanish when choosing a weaker truncation, i.e. large l. Already choosing a truncation of $l = 2$ is a significant improvement. Furthermore improvement with $l = 3$ is marginal.

For the next comparison, the charge pair is not set at the rim, but at the center. The scene is sketched in Figure 4. The continuum theory has translational invariance. Since moving the charge
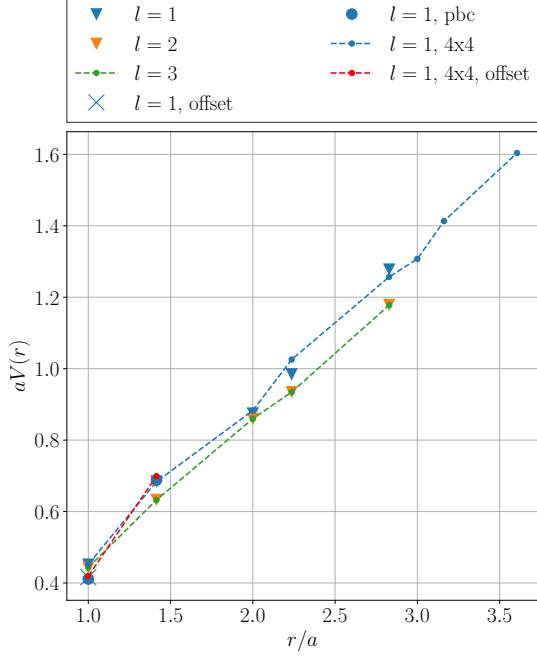
Figure 3: Quark-Antiquark potential for different but comparable setups at $g = 1$. By default 3×3 dimensions and no PBC, if not stated otherwise.

pair away from the rim gives approximate translational invariance, the lattice converges to the continuum theory. The normal setup is used for our initial calculation with $l = 1$ at $r = 1$ (upside down triangle). The potential of the offset setup is now depicted by the blue cross in Figure 3. Unfortunately the lattice is too small, such that no other distances are really feasible. Thus there is no real comparison possible.
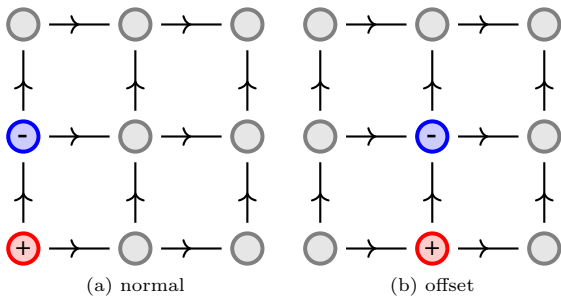
Figure 4: 3×3 lattice with two charge pairs of same distance but different position.

A clever way to avoid rims, is to use periodic boundary conditions (PBC). The disadvantage is that the shortest path is not always the path through the center links, but through the links that are introduced by the PBC. This limits our possible charge pair setups, since already for a 3×3 lattice with PBC, there are only two different setups. All other setups can be created by translation and rotation of those two. They are depicted in Figure 5 Since there is translational invariance, the continuum theory should be approached. Even though it is translational invariance, it is not the same as in the continuum limit, since with PBC the paths also loop around. Those paths are also colored in Figure 5. This should again introduce lattice fragments. The resulting potentials are marked with circles in Figure 3. There is no real influence to be seen.
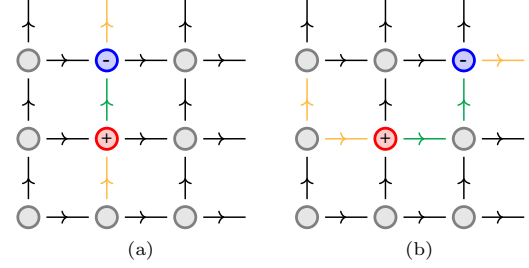

Figure 5: Two 3×3 lattices with PBC and a charge pair with shortest distance (a) and second shortest distance (b). Colored paths: shortest (Green) and second shortest (Yellow) path.

For the continuation of the previous comparison a 4×4 setup is now being used. Again, the charge pair is centered, as shown in Figure 6. Also, only two setups are possible, where no charge is at the rim. All other can be obtained by rotating the lattice. Since translational invariance is approached, lattice fragments should vanish. The potential is marked with a dashed red line in Figure 3. Again, the small number of different charge pair configurations, gives no real comparison to the other data points. No significant change can be observed.

Using the greater lattice size of the 4×4 lattice, the first analysis, where one charge is placed at the lower left corner and the opposite charges
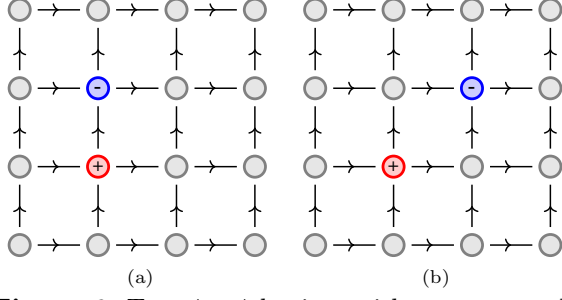
Figure 6: Two 4 × 4 lattices with two centered charge pairs with shortest distance (a) and second shortest distance (b).

at desired distances, can be extended. The resulting potentials a depicted with a blue dashed line. Though the charges a still placed at the rim, an improvement can be seen, as the data points increase in linearity.

At last a variation of the coupling is done. Already little deviations from the original coupling of $g = 1$ show new behaviours. Therefore the potentials with $g = 0.5$, $g = 0.1$ and $g = 5$ are compared to the original. First $g = 5$ is computed with the result in Figure 7. The linearity of the potential starts to vanish and instead steps emerge, which shows that for strong coupling the lattice fragments are intensified. There is no separation between the different setups. This is due to the fact, that at this strong coupling regime the theory starts to break down and very weak truncation or large lattices are needed, to be significant. After strong couplings, weak couplings are now considered. The coupling $g = 0.5$ is computed with the results in Figure 8. A large separation of the potentials is seen, which shows that this coupling is in appropriate regime for this lattice, such that the approach to continuity is relevant.

With decreasing the coupling even more to $g = 0.1$, Figure 9 is obtained. Here a coupling regime is reached, where the lattice size fails to describe the continuum theory not even in a approximation. Neither the weakening in truncation to $l = 2$ or $l = 3$, nor the centering is relevant. Only the 4×4 with offset and the PBC lattice show the capability to be somewhat usable, to approach continuum theory.
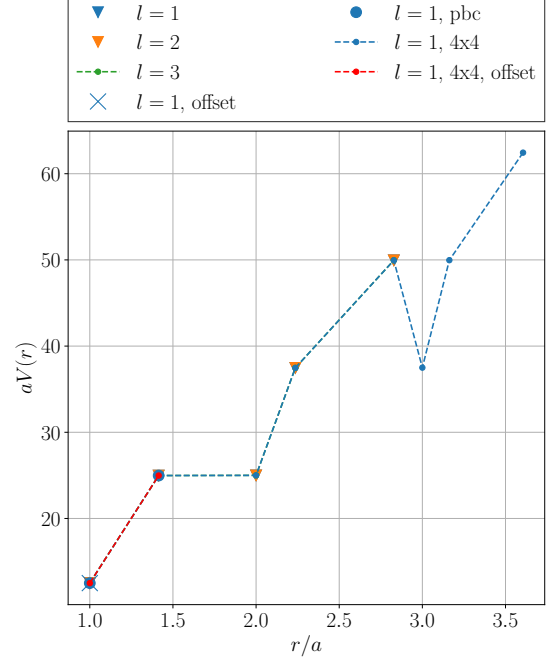

Figure 7: Quark-Antiquark potential at $g = 5$. By default 3 × 3 dimensions and no PBC, if not stated otherwise.
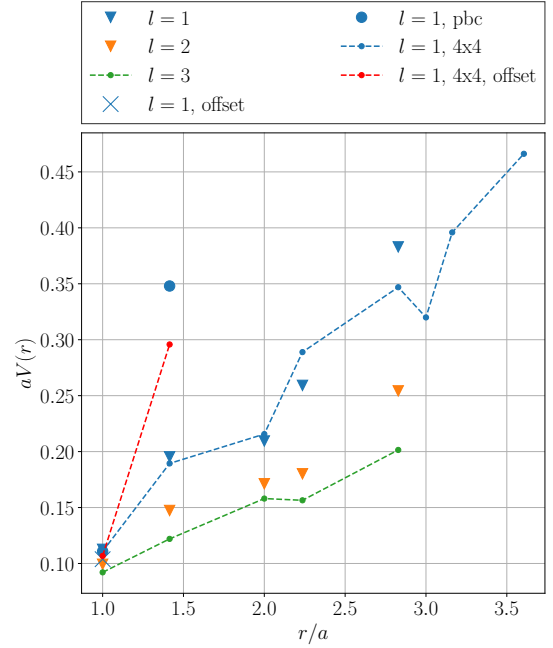

Figure 8: Quark-Antiquark potential for different but comparable setups at $g = 0.5$. By default 3 × 3 dimensions and no PBC, if not stated otherwise.
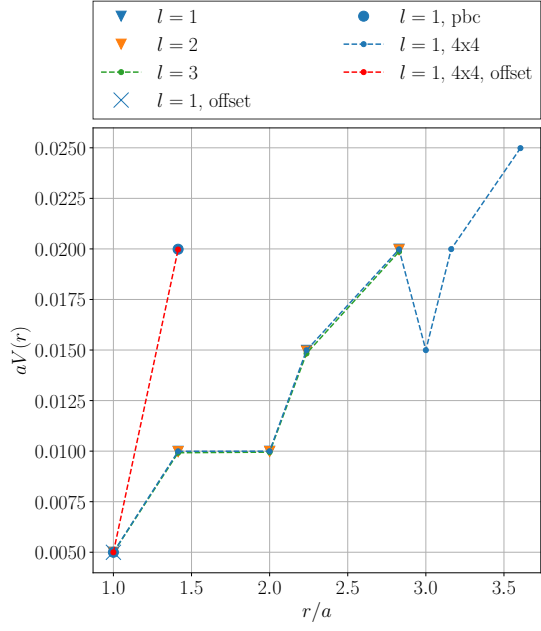
8

Figure 9: Quark-Antiquark potential for different but comparable setups at $g = 0.1$. By default 3×3 dimensions and no PBC, if not stated otherwise.

6 Outlook

Following the analysis of this work, the next step is to determine the running coupling, via e.g. the step scaling approach.[8]

Furthermore the unit scale of the calculated quantities should be determined. Unfortunately this is not really possible for this $(2 + 1)$ dimensional system, since we need to match experimental data which is measured in the real world within a $(3 + 1)$ dimensional field theory.

To give the Hamiltonian formulation of lattice gauge theory a future, where it can be used for larger lattices, the theory needs to be implemented on a quantum computer.[8] The theory can also be implemented using tensor networks.[9, 10]

However the Hamiltonian formulation will be implemented, it is a necessery tool for computations, where so far the dominent method of MCMC simulations of the Lagrangian formulation has the sign problem. [3]

7 Conclusion

With the advancement of quantum computers, the Hamiltonian formulation of gauge theories gains interest again. For this a lattice in the compact U(1) formulation was constructed, where electric and link operators were placed on the links and static charges on the sites. The Kogut Susskind Hamiltonian was modified to be in pure gauge, such that there are no fermionic fields. A truncation l was introduced to render the configuration Hamiltonian finite. Furthermore Guass's Law was used to limit the total number of configuration states to a physical subspace that later on reduces needed computational resources.

With this theoretical setup the numerical implementation started by calculating the matrix elements for the electric and magnetic Hamiltonian. The electric basis and the fact that the link operator is the canonical conjugate of the electric operator was used to obtain the action of the operators on the states. This work briefly dived into computational resources and build an intuition for the needed computation times.

The plaquette expectation value was calculated and compared with scientific literature for confirmation of the correctness of the setup. Finally the quark-antiquark potential was computed by placing two static charges. The potential in

respect to charge to charge distance was calculated, while confinement emerged. Furthermore the influence of different lattices on the potential was discussed by varying the truncation, lattice size and by introduction of periodic boundary conditions.

References

[1] Feynman, R.P.: Simulating physics with computers. International Journal of Theoretical Physics **21**(6), 467–488 (1982) https://doi.org/10.1007/BF02650179

[2] Bañuls, M.C., Blatt, R., Catani, J., Celi, A., Cirac, J.I., Dalmonte, M., Fallani, L., Jansen, K., Lewenstein, M., Montangero, S., Muschik, C.A., Reznik, B., Rico, E., Tagliacozzo, L., Van Acoleyen, K., Verstraete, F., Wiese, U.-J., Wingate, M., Zakrzewski, J., Zoller, P.: Simulating lattice gauge theories within quantum technologies. The European Physical Journal D **74**(8), 165 (2020) https://doi.org/10.1140/epjd/e2020-100571-8

[3] Garofalo, M., Hartung, T., Jakobs, T., Jansen, K., Ostmeyer, J., Rolfes, D., Romiti, S., Urbach, C.: Testing the SU(2) lattice Hamiltonian built from S_3 partitionings. PoS **LATTICE2023**, 231 (2024) https://doi.org/10.22323/1.453.0231

[4] Kogut, J.B.: An introduction to lattice gauge theory and spin systems. Rev. Mod. Phys. **51**, 659–713 (1979) https://doi.org/10.1103/RevModPhys.51.659

[5] Kogut, J., Susskind, L.: Hamiltonian formulation of wilson's lattice gauge theories. Phys. Rev. D **11**, 395–408 (1975) https://doi.org/10.1103/PhysRevD.11.395

[6] Meurer, A., Smith, C.P., Paprocki, M., Certík, O., Kirpichev, S.B., Rocklin, M., Kumar, A., Ivanov, S., Moore, J.K., Singh, S., Rathnayake, T., Vig, S., Granger, B.E., Muller, R.P., Bonazzi, F., Gupta, H., Vats, S., Johansson, F., Pedregosa, F., Curry, M.J., Terrel, A.R., Roučka, v.p., Saboo, A., Fernando, I., Kulal, S., Cimrman, R., Scopatz, A.: Sympy: symbolic computing in python. PeerJ Computer Science **3**, 103 (2017) https://doi.org/10.7717/peerj-cs.103

[7] Virtanen, P., Gommers, R., Oliphant, T.E., Haberland, M., Reddy, T., Cournapeau, D., Burovski, E., Peterson, P., Weckesser, W., Bright, J., van der Walt, S.J., Brett, M., Wilson, J., Millman, K.J., Mayorov, N., Nelson, A.R.J., Jones, E., Kern, R., Larson, E., Carey, C.J., Polat, İ., Feng, Y., Moore, E.W., VanderPlas, J., Laxalde, D., Perktold, J., Cimrman, R., Henriksen, I., Quintero, E.A., Harris, C.R., Archibald, A.M., Ribeiro, A.H., Pedregosa, F., van Mulbregt, P., SciPy 1.0 Contributors: SciPy 1.0: Fundamental Algorithms for Scientific Computing in Python. Nature Methods **17**, 261–272 (2020) https://doi.org/10.1038/s41592-019-0686-2

[8] Crippa, A., Romiti, S., Funcke, L., Jansen, K., Kühn, S., Stornati, P., Urbach, C.: Towards determining the (2+1)-dimensional Quantum Electrodynamics running coupling with Monte Carlo and quantum computing methods (2024). https://arxiv.org/abs/2404.17545

[9] Wu, Y., Liu, W.-Y.: Accurate Gauge-Invariant Tensor Network Simulations for Abelian Lattice Gauge Theory in (2+1)D (2025). https://arxiv.org/abs/2503.20566

[10] Singh, S., Pfeifer, R.N.C., Vidal, G.: Tensor network states and algorithms in the presence of a global u(1) symmetry. Physical Review B **83**(11) (2011) https://doi.org/10.1103/physrevb.83.115125